

## Angular Distributions of Fast Electrons, Ions, and Bremsstrahlung $x/\gamma$ -Rays in Intense Laser Interaction with Solid Targets

Z.-M. Sheng,<sup>1</sup> Y. Sentoku,<sup>1</sup> K. Mima,<sup>1</sup> J. Zhang,<sup>2</sup> W. Yu,<sup>3</sup> and J. Meyer-ter-Vehn<sup>4</sup>

<sup>1</sup>*Institute of Laser Engineering, Osaka University, 2-6 Yamada-oka, Suita, Osaka 565-0871, Japan*

<sup>2</sup>*Laboratory of Optical Physics, Institute of Physics, Chinese Academy of Science, Beijing 100080, China*

<sup>3</sup>*Shanghai Institute of Optics and Fine Mechanics, Shanghai 201800, China*

<sup>4</sup>*Max-Planck-Institut für Quantenoptik, D-85748 Garching, Germany*

(Received 3 April 2000)

We study the angular distributions of fast electrons, ions, and bremsstrahlung  $x/\gamma$ -rays generated during the interaction of an ultrashort intense laser pulse with solid targets. A relation is found on the angular directions for fast electrons and ions as a function of the particle's kinetic energy, experienced Coulomb potential changes, and the incident angle of the laser pulse. It is valid independent of the acceleration mechanisms and the polarization of the laser pulse, as confirmed by particle-in-cell simulations. The angular distribution of bremsstrahlung  $x/\gamma$ -rays is presented to show explicitly its correlation with the corresponding angular distributions of electrons.

PACS numbers: 52.40.Nk, 52.25.Nr, 52.25.Tx, 52.65.Rr

Fast electrons and ions generated in the interaction of ultrashort intense laser pulses with solid and gas targets play a key role for the various applications of intense lasers, such as the fast ignitor of fusion targets, ultrashort  $x/\gamma$ -ray sources, and laser induced nuclear processes, etc. Depending upon the target types (solid or gas), plasma parameters (scale length, density, etc.) and the laser intensities, fast electrons can be produced through vacuum heating [1], plasma wave excitation, and breaking through resonance absorption and electron parametric instabilities [2–5], ponderomotive force acceleration [6,7], and recently proposed direct laser acceleration for electrons inside self-focusing channels [8]. Ions are mainly accelerated by the induced electrostatic fields in recent experiments [6,9,10]. Currently, the angular distributions of fast electrons, ions, and  $x/\gamma$ -ray emissions have been the subject of experimental and theoretical studies in several groups [11–18]. As is obvious, it is one of the important issues for these proposed applications. In this Letter, we present a theory on the angular directions of fast electrons and ions generated in laser-solid interactions, supported by numerical simulation using a 1D3V particle-in-cell (PIC) code. The angular distributions of bremsstrahlung  $x/\gamma$ -rays, obtained by the Monte Carlo method using PIC simulation results, show explicitly the correlation with the angular distributions of electrons.

We consider a geometry shown in Fig. 1 where a planar laser pulse is incident at angle  $\alpha$  onto a solid target. The target is modeled with an electrostatic field around the target surface. As a result, the Hamiltonian of electrons normalized by  $mc^2$  is  $H = [1 + (\mathbf{P} + \mathbf{A})^2]^{1/2} - \Phi$ , where  $\mathbf{P} = \mathbf{p} - \mathbf{A}$  is the canonical momentum normalized by  $mc$ ,  $\mathbf{A}(x, y, t)$  and  $\Phi(x, t)$  are the vector potential of the laser field and scalar potential associated with the electrostatic field, respectively, both normalized by  $mc^2/e$ , and  $m$  the rest mass of electrons. For convenience, we

normalize  $x$  and  $y$  by  $c/\omega_0$  and  $t$  by  $\omega_0^{-1}$  with  $\omega_0$  the laser frequency. Assuming the laser is reflected specularly from the target, the vector potential on the left region of the targets can be written as  $\mathbf{A}(x, y, t) = \mathbf{A}(x, \eta)$ , which includes both the incident and reflected laser fields; here  $\eta = (ck_0/\omega_0)y \sin(\alpha) - t$  with  $ck_0/\omega_0 = 1$  by ignoring the dispersion of laser pulse in preplasma. Using the canonical transform,  $F_2 = \eta P_\eta$ , one finds  $P_y = P_\eta \sin(\alpha)$  and the new Hamiltonian:  $\bar{H} = \gamma - P_\eta - \Phi$ . If electron energy changes in a time scale much shorter than the scalar potential [19],  $\bar{H}$  is an adiabatic constant of motion. If particles are at rest before the interaction and  $\Phi = \Phi_0$ , one has  $\bar{H} = 1 - \Phi_0$ . When the laser pulse leaves the target region, one obtains  $\mathbf{P} = \mathbf{p}$ . Assuming  $p_z = 0$ , generally true both for  $P$  and  $S$  polarization, defining  $\tan(\theta) = p_y/p_x$ , and making use of the adiabatic  $\bar{H}$  and the definition  $\gamma = (1 + p_x^2 + p_y^2)^{1/2}$ , we obtain

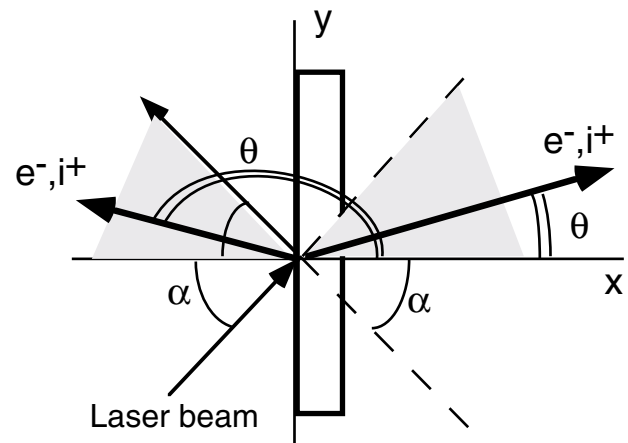


FIG. 1. Schematic drawing of the laser-target interaction geometry shows the equivalence of target interaction with two intersecting laser pulses.

$$\tan(\theta) = \pm \left[ \frac{2(\gamma - 1)(1 + \delta\Phi) - \delta\Phi^2}{(\gamma - 1 - \delta\Phi)^2} \sin^{-2}(\alpha) + \tan^{-2}(\alpha) \right]^{-1/2}, \quad (1)$$

where  $\delta\Phi = \Phi(x, t) - \Phi_0$ . It shows that the angular directions of individual electrons are simply related with their kinetic energy and the experienced Coulomb potential changes. Equation (1) is valid only for electrons. For ions, one needs to replace  $\delta\Phi$  with  $-(Zm/M)\delta\Phi$  in Eq. (1), where  $Z$  and  $M$  are the charge and rest mass of ions, respectively. Since electrons are relatively easy to escape from the target during and after the interaction with laser pulses, the target is usually positively charged. Thus we have  $\delta\Phi > 0$  for all particles. Figures 2(a) and 2(b) show the angular directions of forward moving electrons and ions as a function of their kinetic energy under some given Coulomb potential changes, respectively. It shows that electrons/ions at the same kinetic energy can be found in different angular directions if they experience different Coulomb potential changes. The Coulomb fields tend to *reduce* the ejecting angles of electrons and to *enhance* the angles of ions. Electrons with  $\gamma < 1 + \delta\Phi$  are trapped by the Coulomb potential; when  $\gamma > 1 + \delta\Phi$ , electrons can escape at angles between  $0^\circ$  and  $\alpha$  in the forward direction, or between  $180^\circ$  and  $180^\circ - \alpha$  in the backward direction. Angular directions between  $\alpha$  and  $180^\circ - \alpha$  are forbidden. Energetic electrons with  $\gamma \gg 1 + \delta\Phi$  are found at angles close to the laser direction of incidence and reflection; since the value of  $\gamma$  for ions is usually close to 1, the corresponding angle  $\theta$  is small, about a few degrees for  $\gamma < 1.1$ . In normal incidence  $\alpha = 0^\circ$ , one obtains  $\tan(\theta) = 0$  no matter what values  $\gamma$  and  $\delta\Phi$  take. It means that particles at any energy are directed either in  $0^\circ$  or  $180^\circ$ . When  $\delta\Phi = 0$ , Eq. (1) reduces to

$$\tan(\theta) = \pm \left[ \frac{2}{\gamma - 1} + \frac{\gamma + 1}{\gamma - 1} \tan^{-2}(\alpha) \right]^{-1/2}. \quad (2)$$

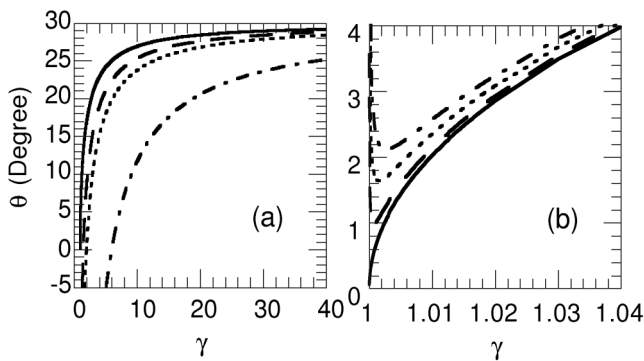


FIG. 2. Angular directions of electrons (a) and ions (b) as a function of particle energy at various electrostatic potential levels when  $\alpha = 30^\circ$ . In (a)  $\delta\Phi = 0$  for —, 0.5 for ---, 1.0 for ···, and 5.0 for - · - ·; in (b)  $\delta\Phi = 0$  for —, 1.0 for ---, 3.0 for ···, and 5.0 for - · - ·.

This is equivalent to a relation proposed for single electrons scattered in two intersecting laser beams in vacuum [20]. It also extends the scattering formula for electrons by single laser beams in vacuum or tenuous plasma (which is recovered when  $\alpha = 90^\circ$ ) [7,12]. Alternatively, Eq. (2) can be rewritten as  $\sin(\theta) = [(\gamma - 1)/(\gamma + 1)]^{1/2} \sin(\alpha)$ , a relation derived earlier by assuming that the momentum is conserved along the target surface between the absorbed photons and accelerated electrons [18].

To confirm the validity of Eq. (1), we performed numerical simulations for laser interaction with a solid target using a 1D3V PIC code accommodated in the Lorenz-boosted frame for oblique incidence of laser pulses [21]. We use targets composed of a high density region at  $5n_c$  with width  $d = (3 \sim 8)\lambda$  and preformed plasma which decreases exponentially with scale length  $L = 0 \sim 3\lambda$  from the high density platform, where  $n_c$  and  $\lambda$  are the critical density and laser wavelength in vacuum, respectively. The ions are protons with a mass ratio  $M/m = 1836$  and  $Z = 1$ . The temporal profile of the laser pulse is  $f(t) = \sin^2(\pi t/t_0)$  for  $0 \leq t \leq t_0$ . Usually, we take  $t_0 = 50\tau$  with  $\tau$  the oscillating period of the pulse.

Initially before the laser interaction, the angular distributions of electrons are homogeneous in all directions between  $0^\circ$  and  $360^\circ$ . During the interaction, the angular distributions evolve into anisotropic ones with time owing to the quiver motion and acceleration of electrons in the laser fields. After the reflection of the laser pulse, electrons move only in the induced electrostatic fields. Figure 3(a) is a typical phase-space plot in angle-energy space (called angular distribution in the following) for all electrons after the laser pulse is fully reflected and leaves the target region. As shown, fast electrons move in the angular direction between  $0^\circ$  and  $\theta(\gamma)$  in the forward direction and between

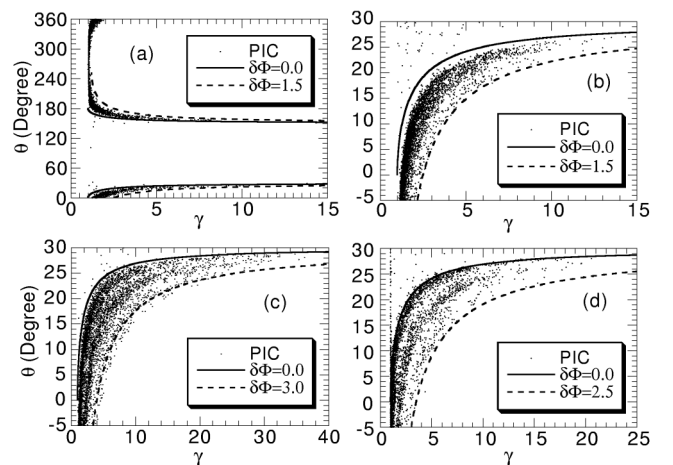


FIG. 3. Angular distributions of electrons after the interaction of a laser pulse (with peak amplitude  $a_0 = 3$ ,  $t_0 = 50\tau$ , and  $\alpha = 30^\circ$ ) with a solid target. The density scale length is (a)  $L = 0$ , (b)  $L = 0.2\lambda$ , (c)  $L = 3\lambda$  for  $p$ -polarized incidence, and (d)  $L = 3\lambda$  for  $s$ -polarized incidence of the laser pulse. The solid and dashed lines are obtained from Eq. (1).

$180^\circ$  and  $180^\circ - \theta(\gamma)$  in the backward direction, where  $\theta(\gamma)$  is given by Eq. (2). Since we use a relatively thin target with  $d = 3\lambda$ , all electrons are pushed in the laser fields and induced electrostatic fields. As a result, few electrons are found in the angular direction between  $30^\circ$  and  $150^\circ$ , which are forbidden according to Eqs. (1) and (2). In Figs. 3(b)–3(d), we show the angular distributions of forward moving electrons for different density scale lengths and laser polarizations. For  $L = 0$ , the main acceleration mechanism is vacuum heating [1]; for  $L = 0.2\lambda$ , plasma wave excitation and wave breaking through resonance are dominant for the observed fast electrons [2,3], while for  $L = 3\lambda$ , parametric excitation of plasma wave and wave breaking around the quarter critical density play a dominant role both for  $P$  and  $S$ -polarized light. In spite of these different mechanisms and laser polarization, electrons are found in angular directions  $\theta(\gamma, \delta\Phi)$  given by Eq. (1), where  $0 \leq \delta\Phi \leq \delta\Phi_{\max}$ . Equation (1) gives the high boundary when  $\delta\Phi = 0$  and the low boundary when  $\delta\Phi = \delta\Phi_{\max}$ . Electrons with the same energy may move in different directions when they have experienced different Coulomb potentials during acceleration. In simulations changing various parameters,  $\delta\Phi_{\max}$  is found to be closely related with the laser absorption in the target. We find that

$$\delta\Phi_{\max} \approx C(\eta_{\text{abs}} a_0^2 t_0)^{1/2}, \quad (3)$$

where  $\eta_{\text{abs}}$  is the total absorption rate (which is also a function of laser intensities, polarizations, and plasma scale lengths),  $t_0$  is the pulse duration, and  $C$  is a constant around unity when  $t_0$  is in units of 50 laser cycles. Moreover, we find that the temperature of hot electrons  $T_h$  scales linearly with  $\delta\Phi_{\max}$ . Since the hot electron energy  $n_h T_h \sim \eta_{\text{abs}} a_0^2 t_0$ , one expects that the number of hot electrons  $n_h$  also scales like  $\delta\Phi_{\max}$ . This proves to be true in our simulations. With the scaling of  $\delta\Phi_{\max}$ , one can predict angular distributions of electrons by measuring the absorption rate. In Fig. 3(b), for example, we find that  $\delta\Phi_{\max} \approx 1.5$  when fitting the simulation result with Eq. (1), which is just close to the value  $\eta_{\text{abs}}^{1/2} a_0$  found in the simulation. One notes that  $\delta\Phi_{\max}$ , though proportional to, is not equivalent to the maximum Coulomb potential found in the simulation box.

Angular distributions of ions shown in Fig. 4 are obtained for similar parameters as for Fig. 3 at a time when the laser pulse is reflected and leaves the target region. They can be well described by Eq. (1) modified for ions as stated before with  $0 < \delta\Phi < \delta\Phi_{\max}^i$ . Usually  $\delta\Phi_{\max}^i > \delta\Phi_{\max}$  ( $\delta\Phi_{\max}^i \approx 1.7\delta\Phi_{\max}$  in this simulation, for example) because ions move at lower velocities and remain relatively localized as compared to electrons. With the increase of laser power, both the kinetic energy of ions and their ejecting angles increase as shown in Fig. 4(d). The nonzero ejecting angle or momentum component along the target surface indicates explicitly that there is a momentum transfer from laser to ions via the ponderomotive force in

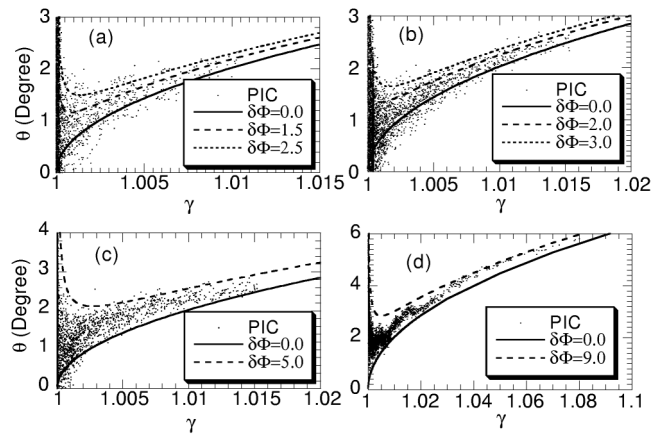


FIG. 4. Angular distributions of forward moving ions after the interaction of a laser pulse (with  $t_0 = 50\tau$  and  $p$  polarization with  $\alpha = 30^\circ$ ). The density scale lengths are (a)  $L = 0$ , (b)  $L = 0.2\lambda$ , (c)  $L = 3\lambda$  with pulse amplitude  $a_0 = 3$ , and (d)  $L = 3\lambda$  with  $a_0 = 10$ . The solid and dashed lines are obtained from Eq. (1) with  $\delta\Phi$  replaced by  $-(Zm/M)\delta\Phi$ .

addition to the acceleration by electrostatic fields along the normal to the target surface.

Now let us compare Eqs. (1) and (2) with some related experiment and 2D PIC simulation results. For example, in an experiment [14], one observed fast electron jets with energy around 170 KeV ( $\gamma = 1.33$ ) in an angular direction about  $\theta = 11^\circ$  when the incident angle  $\alpha = 45^\circ$ . At the same energy, Eq. (2) gives  $\theta = 15.4^\circ$  when the electrostatic field is not considered, which slightly overestimates the angle direction. Taking into account this field, the experimental result is reproduced by Eq. (1) with  $\delta\Phi = 0.1$ . In recent 2D PIC simulations [18], electron jets with  $\gamma \approx 3.0$  are found in  $\theta = 16.7^\circ$  when the incident angle of the laser pulse  $\alpha = 28.9^\circ$ . We find that Eq. (2) gives  $\theta = 20^\circ$  and Eq. (1) gives the 2D simulation result with  $\delta\Phi = 0.32$ .

We notice that, although Eqs. (1) and (2) are obtained for plane laser pulses, primary numerical study on single electrons interacting with two intersecting Gaussian beams in vacuum shows that Eq. (2) is essentially valid for focused beams. Other 2D/3D effects which may modify the angular distributions include the quasistatic magnetic field generation, laser self-focusing, and hole boring. While it is difficult to delineate clearly how the magnetic field would affect the angular distributions of fast electron flows, generally one expects that it tends to reduce the width of angular distributions due to magnetic field pinching. On the other hand, the generation of return currents may lead to the development of Weibel and filamentation instabilities, which could ultimately result in multi-peaked emissions as pointed out in [16]. This may happen in cases with high laser intensities such as  $10^{19}$  W/cm<sup>2</sup> or higher and long plasma scale lengths ensuring efficient absorption of laser energy and large  $n_h T_h$  values. This effect is, however, not expected to be significant in laser interaction with thin targets. The hole-boring effect could break our assumption

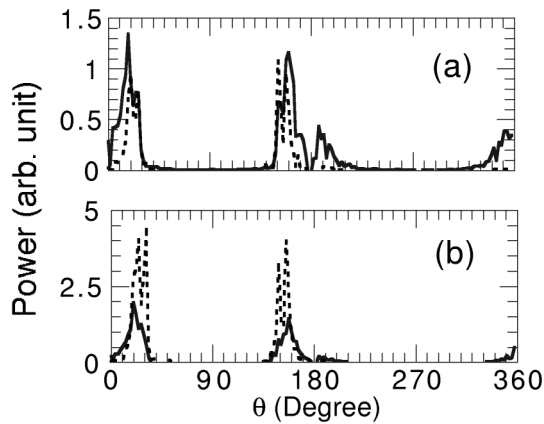


FIG. 5. Angular distributions of x-ray bremsstrahlung for a laser pulse with the same parameters as in Fig. 3 and with plasma scale lengths (a)  $L = 0$  and (b)  $L = 3\lambda$  for  $p$ -polarized incidence. The solid and dashed lines are for bremsstrahlung between 0.01–0.5 MeV and 0.5–30 MeV, respectively.

of specular reflection and introduce a self-focusing effect [8] when  $UT > R$ , where  $U$  is the hole-boring velocity given in [6] with modification taking into account the incident angle,  $T$  the pulse duration, and  $R$  the beam radius. Thus, this effect will not be significant for subpicosecond pulses with intensity less than  $10^{19}$  W/cm<sup>2</sup> and radius sizes around  $R \approx 5 \mu\text{m}$ .

The angular distributions of electrons are closely related to the angular distribution of the bremsstrahlung x/ $\gamma$ -rays. We calculate the bremsstrahlung by use of the Monte Carlo method by postprocessing the distributions of electron momenta obtained from PIC simulations [22]. Example results are given in Fig. 5. It shows that, when  $L = 0$ , there are two forward-radiation peaks around  $\theta = 0^\circ$  (or  $360^\circ$ ) and  $30^\circ$ , respectively, for radiation between 10 keV and 0.5 MeV. Radiation with higher energy between 0.5 and 30 MeV is only found around  $30^\circ$  near which high energy electrons are directed. The angular distribution for the backward radiation is just similar. When  $L = 3\lambda$ , the radiation near  $0^\circ$  is relatively much weaker than around  $30^\circ$ , indicating that electrons are more efficiently accelerated in this case as is evident in Fig. 3. This scale length effect is similar to that found in a recent experiment [16].

In conclusion, a relation on angular directions of electrons and ions is found analytically as a function of the

incident angle of laser pulses, particle kinetic energy, and experienced Coulomb potential changes. It is verified by PIC simulations for a variety of laser pulse and target parameters and is in reasonable agreement with some recent experiments and other simulations. The angular distribution of bremsstrahlung is shown to depend on the energy range of x/ $\gamma$ -rays and the angular distribution of electron energy.

Z. M. S. acknowledges the support of the Japan Society for the Promotion of Science.

- 
- [1] F. Brunel, *Phys. Rev. Lett.* **59**, 52 (1987).
  - [2] W. L. Kruer, *The Physics of Laser Plasma Interaction* (Addison-Wesley, New York, 1988).
  - [3] P. Gibbon and A. R. Bell, *Phys. Rev. Lett.* **68**, 1535 (1992); Th. Schlegel *et al.*, *Phys. Rev. E* **60**, 2209 (1999).
  - [4] E. Esarey *et al.*, *Phys. Rev. Lett.* **72**, 2887 (1994).
  - [5] K. C. Tzeng *et al.*, *Phys. Plasmas* **6**, 2105 (1999).
  - [6] S. C. Wilks *et al.*, *Phys. Rev. Lett.* **69**, 1383 (1992).
  - [7] F. V. Hartemann *et al.*, *Phys. Rev. E* **51**, 4833 (1995); B. Quesnel and P. Mora, *ibid.* **58**, 3719 (1998).
  - [8] A. Pukhov *et al.*, *Phys. Plasmas* **6**, 2847 (1999); C. Gahn *et al.*, *Phys. Rev. Lett.* **83**, 4772 (1999); J. Meyer-ter-Vehn and Z. M. Sheng, *Phys. Plasmas* **6**, 641 (1999).
  - [9] J. Denavit, *Phys. Rev. Lett.* **69**, 3052 (1992).
  - [10] G. S. Sarkisov *et al.*, *Phys. Rev. E* **59**, 7042 (1999).
  - [11] S. Bastiani *et al.*, *Phys. Rev. E* **56**, 7179 (1997).
  - [12] C. I. Moore *et al.*, *Phys. Rev. Lett.* **74**, 2439 (1995); G. Malk *et al.*, *ibid.* **78**, 3314 (1997).
  - [13] M. H. Key *et al.*, *Phys. Plasmas* **5**, 1966 (1998).
  - [14] J. Zhang *et al.*, *Proc. SPIE Int. Soc. Opt. Eng.* **3886**, 332 (1999); P. Zhang *et al.*, *Phys. Rev. E* **57**, R3746 (1998).
  - [15] R. Kodama *et al.*, *Phys. Rev. Lett.* **84**, 674 (2000).
  - [16] M. I. K. Santala *et al.*, *Phys. Rev. Lett.* **84**, 1459 (2000).
  - [17] P. Norreys *et al.*, *Phys. Plasmas* **6**, 2150 (1999).
  - [18] Y. Sentoku *et al.*, *Phys. Plasmas* **6**, 2855 (1999); H. Ruhl *et al.*, *Phys. Rev. Lett.* **82**, 743 (1999).
  - [19] PIC simulation shows that the spectra of the electron density fluctuation and electrostatic field has the highest peak near  $\omega = 0$ ; see also Ref. [18].
  - [20] Z. M. Sheng and J. Meyer-ter-Vehn, in *Superstrong Fields in Plasmas*, edited by M. Lontano *et al.*, AIP Conf. Proc. No. 426 (AIP, Woodbury, 1998), p. 153.
  - [21] R. Lichters *et al.*, *Phys. Plasmas* **3**, 3425 (1996); P. Gibbon *et al.*, *Phys. Plasmas* **6**, 947 (1999).
  - [22] Y. Sentoku *et al.*, *Phys. Plasmas* **5**, 4366 (1998).